AAS 15-343

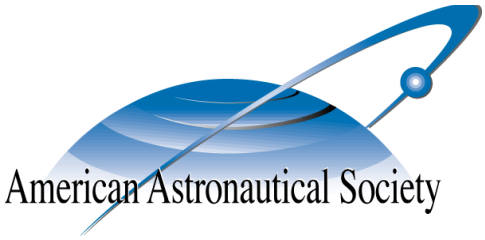

American Institute of
Aeronautics and Astronautics

SPHERICAL MAGNETIC DIPOLE ACTUATOR FOR SPACECRAFT ATTITUDE CONTROL

Joshua Chabot and Hanspeter Schaub

University of Colorado, Boulder

AAS/AIAA Spaceflight Mechanics Meeting

Williamsburg, Virginia **January 11–15, 2015**

AAS Publications Office, P.O. Box 28130, San Diego, CA 92198

(Preprint) AAS 15-343

SPHERICAL MAGNETIC DIPOLE ACTUATOR FOR SPACECRAFT ATTITUDE CONTROL

Joshua Chabot* **and Hanspeter Schaub†**
University of Colorado, Boulder

This paper develops an analytical force and torque model for a spherical magnetic dipole attitude control device, along with a control scheme that includes singularity avoidance. The device proposed consists of a non-contact spherical dipole rotor enclosed in an array of coils that is fixed to the spacecraft body. Excitation of the coils as prescribed by the control law rotates the dipole rotor in such a manner as to produce a desired reaction torque for orienting the spacecraft. The coils also control the rotor's position inside the spacecraft body via a separate control law because of the non-contact nature of the device. Due to the axisymmetric field of the dipole rotor, underactuation is possible with one device and therefore two spherical actuators are needed for full attitude control.

INTRODUCTION

Spacecraft require a minimum of three reaction wheels for full attitude control and often have more for redundancy. The use of spherical actuators, however, could reduce this number, resulting in potential attitude control system mass savings, among other advantages that stem from using a spherical momentum transfer device. Taking advantage of this spherical symmetry provides more control authority from a single device than a reaction wheel can offer.

The design proposed here consists of a spherical dipole magnet (the rotor) surrounded by an array of coils (the stator), as shown in Figure 1. The stator is fixed to the spacecraft body, whereas the rotor is magnetically suspended inside the stator. Electrical current is sent to the array of coils in such a manner as to control the spin of the rotor, along with its position inside the stator. Because the rotor is magnetically suspended, frictional losses are negligible, potentially extending the lifespan of the device compared to conventional reaction wheel systems where failure often comes from mechanical contact. Mechanical contact also introduces vibrations that can be detrimental to the science of a mission. As such, the magnetic levitation of the rotor could eliminate these unwanted vibrations thanks to its non-contact nature and through active vibration damping.[1,2]

Spherical actuators were originally proposed in the early 1960s[3,4,5] and have gained renewed interest in the past decade. As with conventional electric motors, spherical actuator designs fall under two general categories: synchronous and asynchronous. Asynchronous motors utilize a changing magnetic field to induce a current in a nonmagnetic rotor. The induced current interacts with the changing magnetic field to produce a torque. Synchronous motors, on the other hand, rely on the interaction between permanent magnets and electromagnetics, where coil excitation is timed via control logic to produce torque. The actuator proposed here falls under the latter category.

*Masters Student, Department of Aerospace Engineering Sciences, University of Colorado, Boulder, and AIAA Member.
†Professor, Department of Aerospace Engineering Sciences, University of Colorado, Boulder, and AIAA Member.

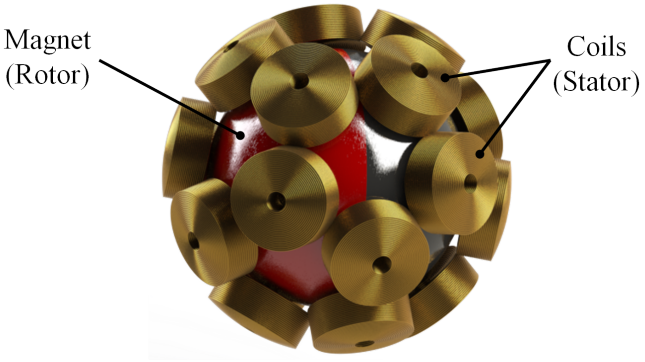

Figure 1: Spherical Dipole Actuator with 20 Coils

The majority of research conducted so far in this area studies asynchronous-type spherical actuators. Early designs propose using a combination of magnetic induction for torque production and electrostatic force for suspending the rotor.[4,5] Later designs move away from using electrostatics due to the large electric potentials and hard vacuums needed and instead rely purely on induced effects for torque and suspension. More recent work focuses on developing models for the induced fields in the rotor,[6,7,8,9,10] and experimental investigations have been conducted to validate these models and move towards real world application.[11,12]

In addition to the work being done with asynchronous actuators, there is currently research into a synchronous spherical actuator design for attitude control that relies on a rotor with eight magnetic poles.[1] Analytical force and torque models for this actuator have been developed and confirmed through experimental investigations[13,2] and finite-element modeling.[14] Also, studies examine optimal stator sensor placement,[14] rotor design optimization,[15] back-EMF modeling,[16] and eddy current losses.[17]

One difficulty with an eight-pole rotor is that it cannot be fabricated from a homogeneous substrate. Instead, it need be an amalgam of smaller dipole magnets that together approximate the desired spherical magnetic field distribution. This poses a potential problem for applications in attitude control because of the high spin rates that are required. Because of this, fabricating such a rotor would require precision machining of magnetic material, likely making the device costly.

The design proposed here instead uses a spherical dipole magnet as a rotor. Spherical dipole magnets are inexpensive, readily available, and produced from a homogeneous substrate. However, unlike an eight-pole rotor, a dipole rotor cannot always provide the desired torque due to its axisymmetry. This potentially limits the attitude control capabilities from a single actuator, or leads to underactuated control strategies. As such, a two actuator configuration is examined here in addition to the single actuator case. Sensing and induced effects are not considered in this work, and are left to future research.

EQUATIONS OF MOTION FOR SPACECRAFT WITH n-SPHERICAL ACTUATORS

The total angular momentum for a spacecraft with n-spherical actuators is simply the sum of the angular momenta of the spacecraft body and the n-spherical actuator rotors,

$$\mathbf{H} = \mathbf{H}_B + \sum_{m=1}^{n} \mathbf{H}_m \tag{1}$$

where $\mathbf{H}_B$ is the spacecraft body angular momentum and $\mathbf{H}_m$ are the spherical actuator momenta. The time rate of change of angular momentum about the system's center of mass is equivalent to the net external torque on the system,

$$\dot{\mathbf{H}} = \dot{\mathbf{H}}_B + \sum_{m=1}^{n} \dot{\mathbf{H}}_m = \mathbf{L} \tag{2}$$

and additionally, each spherical actuator can be treated as a separate system whose angular momentum rate is caused by an external torque:

$$\dot{\mathbf{H}}_m = -\mathbf{u}_m \tag{3}$$

Note that the actuator torque $\mathbf{u}_m$ is negative in this instance because, as will be seen, the actuator torque model describes the torque on the actuator coils, whereas here torque on the rotor is of interest. Eq. (3) can then be substituted into Eq. (2) producing

$$\dot{\mathbf{H}}_B - \sum_{m=1}^{n} \mathbf{u}_m = \mathbf{L} \tag{4}$$

Because $\mathbf{H}_B$ is described in the spacecraft body frame, the transport theorem must be applied to take the inertial derivative:

$$\frac{^{\mathcal{B}}\mathrm{d}}{\mathrm{d}t}(\mathbf{H}_B) + \boldsymbol{\omega}_{\mathcal{B}/\mathcal{N}} \times \mathbf{H}_B - \sum_{m=1}^{n} \mathbf{u}_m = \mathbf{L} \tag{5}$$

From the definition of angular momentum about a rigid body's center of mass and due to the fact that the spacecraft inertia tensor is constant as seen from the spacecraft body frame, Eq. (5) may then be rewritten as

$$[I]\,\dot{\boldsymbol{\omega}}_{\mathcal{B}/\mathcal{N}} + \boldsymbol{\omega}_{\mathcal{B}/\mathcal{N}} \times [I]\,\boldsymbol{\omega}_{\mathcal{B}/\mathcal{N}} = \sum_{m=1}^{n} \mathbf{u}_m + \mathbf{L} \tag{6}$$

where $\boldsymbol{\omega}_{\mathcal{B}/\mathcal{N}}$ is the spacecraft body rate vector with respect to an intertial frame and $[I]$ is the spacecraft inertia tensor. As can be seen from Eq. 6, the torque produced by spherical actuators can be viewed as an external torque on the spacecraft. Additionally, Eq. (3) can be used to derive the equations of motion for the spherical actuators. Since the inertia of a sphere is identical whether viewed in a body or inertial frame, Eq. (3) can be rewritten as

$$[I]_m\,\dot{\boldsymbol{\omega}}_{\mathcal{R}_m/\mathcal{N}} = -\mathbf{u}_m \tag{7}$$

where $[I]_m$ denotes the m^{th} spherical actuator inertia and $\dot{\boldsymbol{\omega}}_{\mathcal{R}_m/\mathcal{N}}$ the m^{th} angular velocity with respect to inertial.

Along with the spacecraft dynamics equations, an attitude parameterization is necessary. Modified Rodrigues Parameters (MRP) are chosen, and the MRP attitude kinematic differential equation is given by

$$\dot{\boldsymbol{\sigma}} = \frac{1}{4}\left[(1 - \boldsymbol{\sigma}^T\boldsymbol{\sigma})I_{3\times3} + 2\tilde{\boldsymbol{\sigma}} + 2\boldsymbol{\sigma}\boldsymbol{\sigma}^T\right]\boldsymbol{\omega} \tag{8}$$

where $\boldsymbol{\sigma}$ is the MRP attitude vector.[18] To avoid the MRP singularity, the norm of $\boldsymbol{\sigma}$ is kept less than or equal to unity by switching to the MRP shadow set when necessary. Finally, the following feedback control law is used to stabilize the spacecraft relative to the attitude origin:

$$\boldsymbol{\tau} = \sum_{m=1}^{n} \mathbf{u}_m = -P\boldsymbol{\sigma} - [D]\boldsymbol{\omega} \tag{9}$$

where P is a positive scalar and $[D]$ is a positive-definite matrix. This attitude regulation control law is globally asymptotically stabilizing if no unmodeled torques are present, which is the case for all simulations presented here.[19,18] Note that the following developments are not tied to this particular choice of attitude control law in Eq. (9). Rather, this proportional-deriviative regulation control can be substituted with any desired attitude control torque expression, including a reference tracking control. Of interest is how this desired control torque $\boldsymbol{\tau}$ is generated through the rotors and coils.

SPHERICAL ACTUATOR MODEL

The development of the force and torque model for the proposed spherical actuator begins by examining the interaction between the rotor and an individual coil. Multiple coordinate frames are defined, as shown in Figure 2, where $\mathcal{B}$ is a spacecraft body-fixed frame, $\mathcal{R}$ is a frame fixed to the dipole rotor and aligned with its axis of magnetization, and $\mathcal{C}_k$ is the k^{th} coil-fixed frame aligned with the axis of the k^{th} coil.

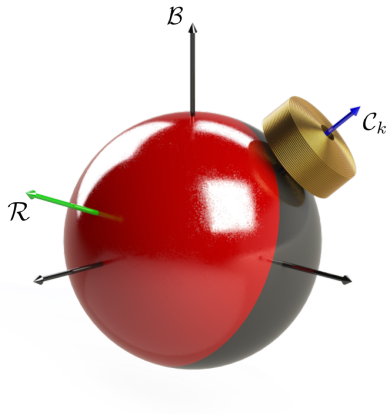

Figure 2: Definition of Coordinate Frames

To find the force and torque on an individual coil caused by the magnetic field of the rotor, the Lorentz force law is first simplified by assuming there are no external electric fields present in the system:

$$\mathrm{d}\mathbf{F}_k = (\rho\mathbf{E} + \mathbf{J} \times \mathbf{B})\,\mathrm{d}V = (\mathbf{J} \times \mathbf{B})\,\mathrm{d}V \tag{10}$$

where $\mathrm{d}\mathbf{F}_k$ is the differential force on the coil current density $\mathbf{J}$ caused by the external magnetic field $\mathbf{B}$. Eq. (10) is modified into a torque expression by taking the cross product between the position vector and the differential force element:

$$\mathrm{d}\mathbf{T}_k = \mathbf{R} \times \mathrm{d}\mathbf{F}_k = \mathbf{r} \times (\mathbf{J} \times \mathbf{B})\,\mathrm{d}V \tag{11}$$

Next, integrating Eqs. (10) and (11) over the volume of the coil yields the total force and torque acting on the coil:

$$\mathbf{F}_k = \int_V \mathbf{J} \times \mathbf{B}\,\mathrm{d}V \tag{12a}$$

$$\mathbf{T}_k = \int_V \mathbf{R} \times \mathbf{J} \times \mathbf{B}\,\mathrm{d}V \tag{12b}$$

These volume integrals can then be expanded into a useful form using spherical components, producing

$$\mathbf{F}_k = \int_{R_a}^{R_b} \int_{\theta_a}^{\theta_b} \int_{-\pi}^{\pi} \mathbf{J} \times \mathbf{B}\, R^2 \sin\theta \,\mathrm{d}\phi \,\mathrm{d}\theta \,\mathrm{d}r \tag{13a}$$

$$\mathbf{T}_k = \int_{R_a}^{R_b} \int_{\theta_a}^{\theta_b} \int_{-\pi}^{\pi} \mathbf{R} \times \mathbf{J} \times \mathbf{B}\, R^2 \sin\theta \,\mathrm{d}\phi \,\mathrm{d}\theta \,\mathrm{d}R \tag{13b}$$

As shown in Figure 3, parameterization with spherical components is convenient since the coil is approximately a section of a sphere delimited by its inner and outer radii, R_a and R_b, its minor and major central angles, θ_a and θ_b, and its angle of revolution, ϕ.

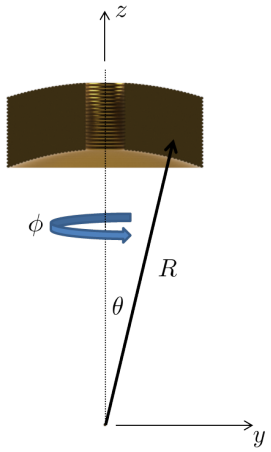

Figure 3: Coil Coordinate Frame

At this point in the development, it's useful to assign coordinate frames to the vectors. Because force and torque on a single coil are being examined, it is beneficial to express Eq. (13) in a local coil frame:

$${}^{c_k}\mathbf{F}_k = \int_{R_a}^{R_b} \int_{\theta_a}^{\theta_b} \int_{-\pi}^{\pi} {}^{c_k}\mathbf{J} \times {}^{c_k}\mathbf{B}\, R^2 \sin\theta \,\mathrm{d}\phi \,\mathrm{d}\theta \,\mathrm{d}r \tag{14a}$$

$${}^{c_k}\mathbf{T}_k = \int_{R_a}^{R_b} \int_{\theta_a}^{\theta_b} \int_{-\pi}^{\pi} {}^{c_k}\mathbf{R} \times {}^{c_k}\mathbf{J} \times {}^{c_k}\mathbf{B}\, R^2 \sin\theta \,\mathrm{d}\phi \,\mathrm{d}\theta \,\mathrm{d}R \tag{14b}$$

where the position vector in the coil frame is

$${}^{c_k}\mathbf{R} = \begin{pmatrix} R\sin\theta\cos\phi \\ R\sin\theta\sin\phi \\ R\cos\theta \end{pmatrix}, \tag{15}$$

and the current density vector is

$${}^{c_k}\mathbf{J} = \frac{i_k N}{A} \begin{pmatrix} -\sin\phi \\ \cos\phi \\ 0 \end{pmatrix} = \frac{2 i_k N}{(R_b^2 - R_a^2)(\theta_b - \theta_a)} \begin{pmatrix} -\sin\phi \\ \cos\phi \\ 0 \end{pmatrix}. \tag{16}$$

In Eq. (16), i_k denotes the k^{th} coil current, N the number of turns in the coil, and A the cross-sectional area of the coil. Additionally, the magnetic field of the dipole rotor is given by

$$ {}^{\mathcal{C}_k}\mathbf{B} = \frac{\mu_0}{4\pi}\left(\frac{3\,{}^{\mathcal{C}_k}\boldsymbol{\rho}({}^{\mathcal{C}_k}\mathbf{m}\cdot{}^{\mathcal{C}_k}\boldsymbol{\rho})}{\rho^5} - \frac{{}^{\mathcal{C}_k}\mathbf{m}}{\rho^3}\right) \tag{17} $$

where $\boldsymbol{\rho}$ is the relative position between a differential coil element and the center of the rotor:

$$ {}^{\mathcal{C}_k}\boldsymbol{\rho} = {}^{\mathcal{C}_k}\mathbf{R} - {}^{\mathcal{C}_k}\mathbf{r} = {}^{\mathcal{C}_k}\mathbf{R} - [\mathcal{C}_k\mathcal{B}]\,{}^{\mathcal{B}}\mathbf{r} \tag{18} $$

Here $\mathbf{r}$ is the position of the rotor with respect to the center of the stator and $[\mathcal{C}_k\mathcal{B}]$ is the rotation matrix that transforms the rotor position from the body frame to the local coil frame. Also to express the rotor's magnetic field in the coil frame, the rotor's magnetic moment vector $\mathbf{m}$ must be transformed:

$$ {}^{\mathcal{C}_k}\mathbf{m} = [\mathcal{C}_k\mathcal{R}]\,{}^{\mathcal{R}}\mathbf{m} \tag{19} $$

Note that the third axis of the rotor frame is aligned with the rotor's axis of magnetization. With everything expressed in the common coil frame, the equations in (14) are integrated yielding the force and torque on a single coil. As it stands now, the integrals in Eq. (14) cannot be solved explicitly and must instead be integrated numerically. However, if the rotor is close to the center of the stator, $\mathbf{r} \ll \mathbf{R}$ and $\boldsymbol{\rho} \to \mathbf{R}$, and with this, analytical solutions to the volume integrals can be found. These algebraic expressions for $\mathbf{F}_k$ and $\mathbf{T}_k$ are provided in the Appendix for reference.

Finally, to get the overall force and torque produced by the spherical actuator given an arbitrary configuration of coils, the forces and torques from each of the coils must be described in the body frame and summed together:

$$ {}^{\mathcal{B}}\boldsymbol{f} = \sum_{k=1}^{n}[\mathcal{B}\mathcal{C}_k]\,{}^{\mathcal{C}_k}\mathbf{F}_k = [\mathrm{K}_F]\,\mathbf{i} \tag{20a} $$

$$ {}^{\mathcal{B}}\boldsymbol{\tau} = \sum_{k=1}^{n}[\mathcal{B}\mathcal{C}_k]\,{}^{\mathcal{C}_k}\mathbf{T}_k = [\mathrm{K}_T]\,\mathbf{i} \tag{20b} $$

where n is the number of coils in the system, $[\mathcal{B}\mathcal{C}_k]$ transforms from the $\mathcal{C}_k$ frame to the $\mathcal{B}$ frame, $[K_F]$ and $[K_T]$ are the $3 \times n$ force and torque characteristic matrices, and $\mathbf{i}$ is the $n \times 1$ coil current vector.[1] If the rotor's position in the stator is accounted for in the derivations, then the characteristic matrices depend on the rotor's position and attitude and must be numerically integrated each time step. This numerical integration is prohibitively time-consuming for real-time application aboard a spacecraft. However, if the rotor is close enough to the center of the stator, then the algebraic characteristic matrices provide a sufficient approximation and can be precomputed offline, allowing for real-time implementation.

SPACECRAFT ATTITUDE CONTROL

Now that the relationships between coil current and actuator force and torque have been found, they are used to calculate the necessary coil current vector given a desired spacecraft torque command. For the case where only a single spherical actuator is used,

$$ \begin{bmatrix} K_T \\ K_F \end{bmatrix}\mathbf{i} = \begin{bmatrix} \boldsymbol{\tau} \\ \boldsymbol{f} \end{bmatrix} \tag{21} $$

relates coil currents to forces and torques. Here, the rotor position control force $\boldsymbol{f}$ is given by a closed-loop feedback control law and converges to zero as the rotor becomes centered in the stator. A simple PD controller is chosen to provide rotor position control:

$$\boldsymbol{f} = -K_P \mathbf{r} - K_D \dot{\mathbf{r}} \tag{22}$$

where K_P and K_D are positive scalar gains. The coil current vector in Eq. (21) can then be found by applying a Moore-Penrose pseudoinverse:

$$\mathbf{i} = \begin{bmatrix} K_T \\ K_F \end{bmatrix}^+ \begin{bmatrix} \boldsymbol{\tau} \\ \boldsymbol{f} \end{bmatrix} \tag{23}$$

Because of the axisymmetry of the dipole rotor, $[K_T]$ is rank 2, and therefore there is a null space of torques that cannot be produced by the single actuator. In instances where a torque cannot be produced, the pseudoinverse finds the least-squares solution to the rank deficient problem. The characteristic force matrix, however, is always full rank and can therefore provide the desired position control force.

With this, a second spherical actuator can be added to the system to remedy the rank deficiency,

$$\begin{bmatrix} K_{T1} & K_{T2} \\ K_{F1} & \mathbf{0} \\ \mathbf{0} & K_{F2} \end{bmatrix} \begin{pmatrix} \mathbf{i}_1 \\ \mathbf{i}_2 \end{pmatrix} = \begin{bmatrix} \boldsymbol{\tau} \\ \boldsymbol{f}_1 \\ \boldsymbol{f}_2 \end{bmatrix} \tag{24}$$

where the subscripts indicate the first and second actuator. The pseudoinverse can again be used to solve for the current vectors,

$$\begin{pmatrix} \mathbf{i}_1 \\ \mathbf{i}_2 \end{pmatrix} = \begin{bmatrix} K_{T1} & K_{T2} \\ K_{F1} & \mathbf{0} \\ \mathbf{0} & K_{F2} \end{bmatrix}^+ \begin{bmatrix} \boldsymbol{\tau} \\ \boldsymbol{f}_1 \\ \boldsymbol{f}_2 \end{bmatrix}. \tag{25}$$

However, now the torque portion of Eq. (25) is rank 4, in general, and the system is overdetermined. The pseudoinverse therefore calculates the minimum current norm solution of the system. Despite this augmented configuration, there are instances where Eq. (25) becomes rank deficient. This occurs when the magnetic moment vectors of the two rotors are parallel, when $[K_{T1}] = [K_{T2}]$. In these instances, the system is equivalent to a single actuator.

To avoid alignment of the rotors, an equal magnitude and opposite sign torque can be applied to each of the rotors that drives them apart, while at the same time inducing no net torque on the spacecraft. This null motion torque is given by the following control law:

$$\mathbf{L}_n = \pm(K_1 \, \Delta\phi + K_2 \, \dot{\phi}) \left(\frac{\mathbf{m}_1 \times \mathbf{m}_2}{|\mathbf{m}_1 \times \mathbf{m}_2|} \right) \tag{26}$$

where K_1 and K_2 are positive scalar gains, $\mathbf{m}_1$ and $\mathbf{m}_2$ are the rotors' respective magnetic moment vectors, and $\Delta\phi$ is the error between the actual and desired angle between the magnetic moment vectors. Note that this null motion control law does not guarantee the rotors will not align. Should the rotors align, Eq. 26 encounters a singularity due to direction ambiguity of the null torque vector.

NUMERICAL SIMULATIONS

For all simulations in this section, the parameters in Table 1 are used. The rotor is assumed to be solid and uniformly magnetized. Additionally, only an 8-coil configuration is used because of the simulation time required when the rotor is not assumed centered.

Table 1: Simulation Parameters

Parameter	Value	Parameter	Value
Number of Coils	8	Rotor Mass	515 g
Windings per Coil, N	100	Rotor Magnetic Moment, $\mathbf{m}$	30.4 $\mathrm{N{\cdot}m/T}$
Inner Coil Radius, R_a	27.5 mm	Spacecraft Inertia, $[I]$	diag([0.2 0.3 0.8]) $\mathrm{kg{\cdot}m^2}$
Outer Coil Radius, R_b	32.5 mm	Initial Attitude, $\boldsymbol{\sigma}$	[-0.0174 -0.1431 0.2053]
Inner Coil Angle, θ_a	5°	Initial Body Rates, $\boldsymbol{\omega}$	[5 -2 3] °/sec
Outer Coil Angle, θ_b	35°	P Gain	0.008 $\mathrm{N{\cdot}m}$
Rotor Radius	25.4 mm	$[D]$ Gain	[0.01 0.01 0.03] $\mathrm{N{\cdot}m{\cdot}sec}$

Validation of Centered Rotor Assumption

As previously mentioned, the volume integrals in Eq. (14) require numerical integration unless the rotor is centered within the stator. For real-time implementation, numerical volume integration is not an option due to its prohibitive computation time. However if the rotor is sufficiently centered, then the analytical solutions to the volume integrals are good approximations, and since the rotor's position is controlled, it will remain close to the center. Figure 4a shows the attitude error between a maneuver with an off-center rotor needing numerical volume integration and the same maneuver with the rotor assumed perfectly centered in the stator, and therefore using the algebraic expressions. As can be seen, there are differences between the two simulations due to the initial offset of the rotor, however the attitude differences are relatively small and converge to zero after the rotor becomes centered. Additionally, Figure 4b displays how the rotor's position converges to center thanks to the position control loop. Rotor position control has been successfully demonstrated, and as such, the rotor will be assumed centered, drastically reducing simulation run time.

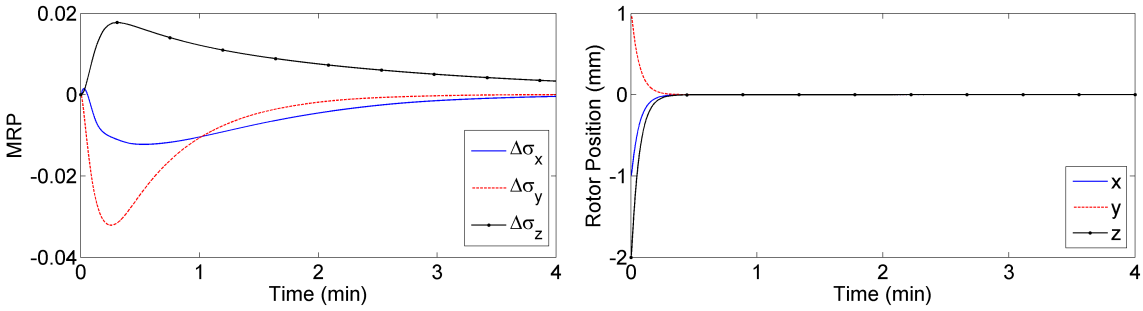

(a) Centered/Off-Center Attitude Error

(b) Rotor Position

Figure 4: Comparison of Centered and Off-Centered Rotor

Single Actuator Attitude Control

Despite its inherent rank deficiency, the single actuator configuration has proven to be effective at detumbling and pointing a spacecraft in numerical simulations conducted so far. Figure 5 illustrates this point showing how the spacecraft attitude and body rate errors converge to zero. Along with this, the rotor's angular velocity converges to a steady-state value, as expected, and is due to the angular momentum originally contained in the spacecraft body. The peak current draw for the device occurs at the beginning of the maneuver and is 130 mA. Further investigation into single actuator attitude control is necessary to fully understand its capabilities and limitations.

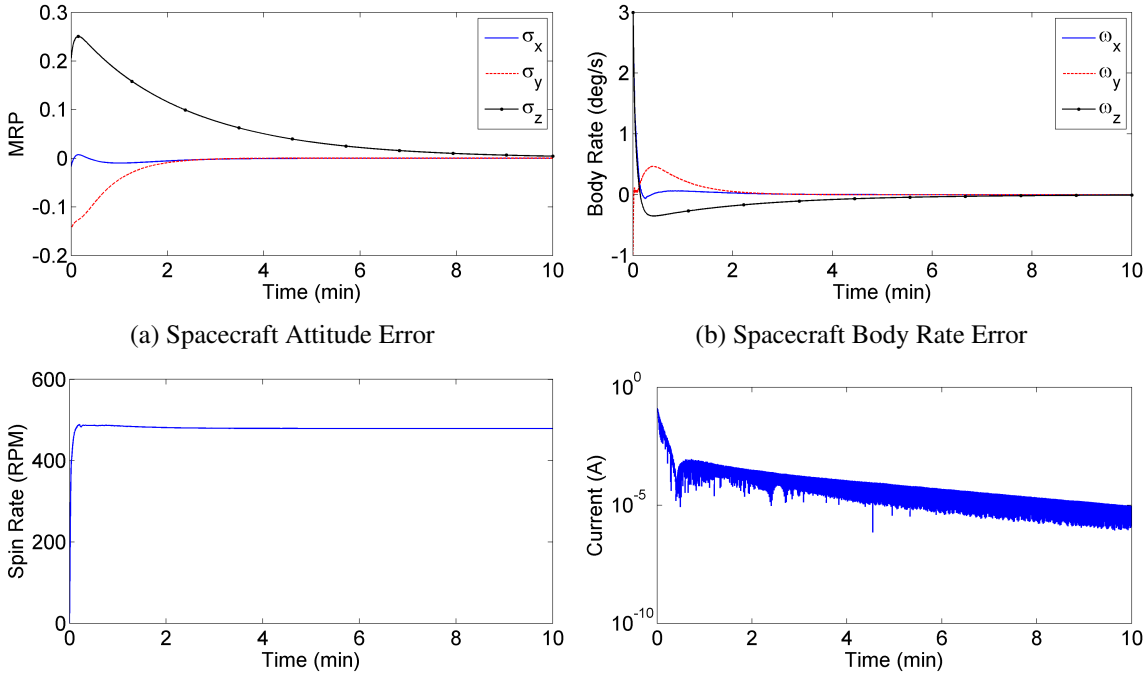

(a) Spacecraft Attitude Error

(b) Spacecraft Body Rate Error

(c) Rotor Angular Velocity

(d) Rotor Total Current Draw

Figure 5: Single Actuator Attitude Control Maneuver

Dual Actuator Attitude Control

Figure 6 displays the same attitude maneuver, now with two spherical actuators. As can be seen, the controller performance is very similar to that which was provided by the single actuator. However, the dual actuator system requires less current to each of the individual rotors and lower total peak current – approximately 107 mA at the beginning of the maneuver. One downside to the dual actuator configuration is that the rotors can end up in a spin configuration with high angular velocities despite relatively low or zero total system angular momentum. This is due to the fact that the angular momenta of the rotors can point in opposite directions, in turn canceling and conserving total angular momentum. Additionally, the spin configuration the two rotors end up in depends on their state at the beginning of the attitude maneuver.

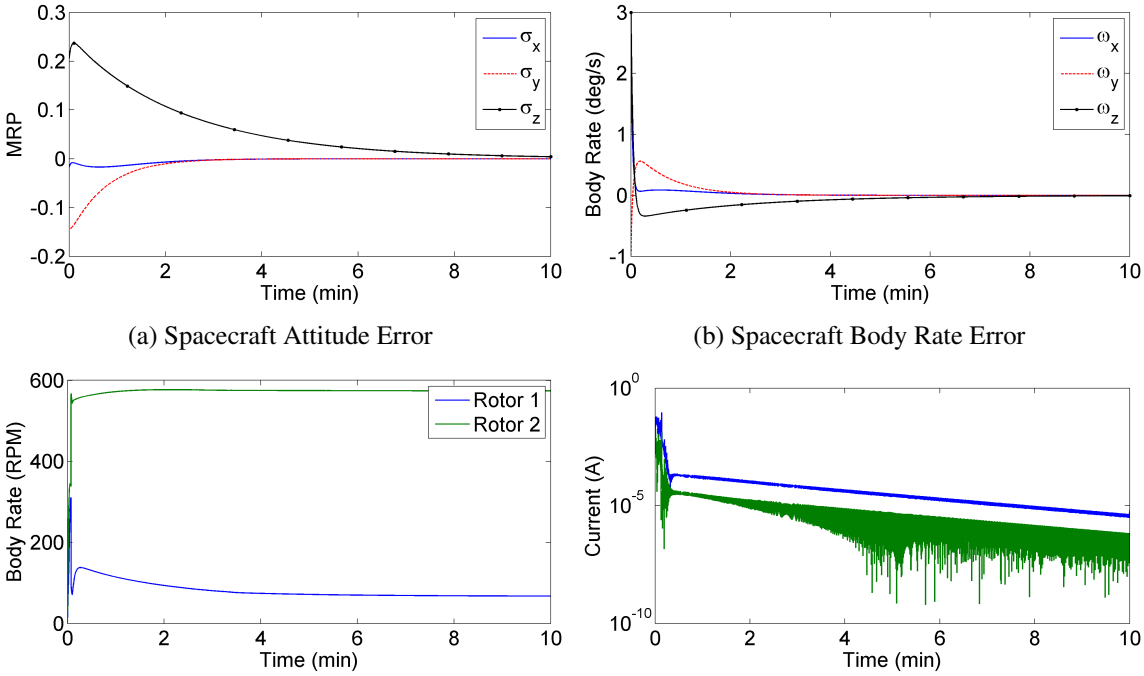

(a) Spacecraft Attitude Error

(b) Spacecraft Body Rate Error

(c) Rotor Angular Velocity

(d) Rotor Total Current Draw

Figure 6: Dual Actuator Attitude Control Maneuver

Null Motion Singularity Avoidance

Applying the singularity avoidance control law presented in Eq. (26) to the dual actuator system does little to the attitude control maneuver examined so far. This is because it is very unlikely for the two actuators to align. Also because the rotors are spinning at high angular velocities, should they come close to aligning, it would only be for an instant. Consequently, it's more illustrative to look at reconfiguring the rotors for maneuver initialization. Figure 7 presents a case where the two rotors are initially nearly aligned. The null motion control law reconfigures them such that their magnetic moment vectors are perpendicular, and does so without imparting a torque on the spacecraft. The control law gains were chosen to be $K_1 = 0.0001\,\mathrm{N\cdot m}$ and $K_2 = 0.0001\,\mathrm{N\cdot m\cdot sec}$.

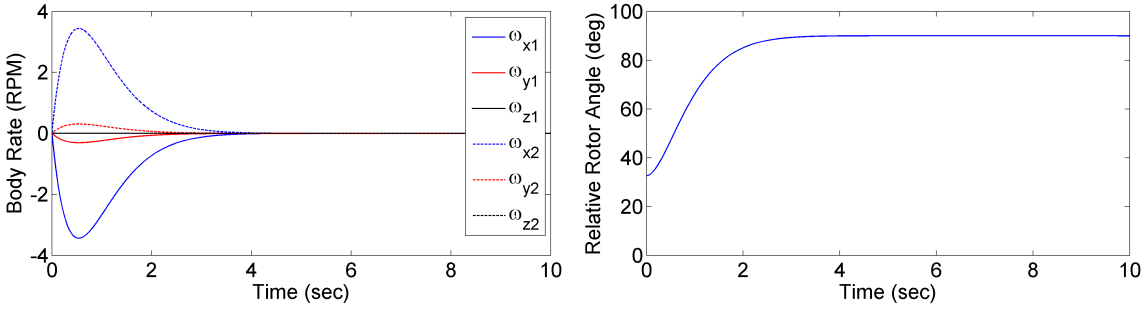

(a) Rotor Angular Velocities

(b) Angle Between Magnetic Moment Vectors

Figure 7: Rotor Reconfiguration Using Null Motion

CONCLUSION

A spherical actuator for spacecraft attitude control has been presented that relies on a simple dipole magnet to exchange momentum with the spacecraft. The equations of motion for this system were derived and numerically simulated showing that the proposed actuator can indeed provide attitude control. A single spherical actuator was first examined and was able to successfully perform an attitude maneuver despite its inability to always produce a desired torque. Further research into this form of underactuated control will be necessary to fully understand how effective a single actuator can be. A dual actuator configuration was also investigated and was found to successfully provide attitude control while also requiring less current than a single actuator. Finally, a null motion control law was developed to avoid singularities and was able to rotate the actuators into a more favorable configuration without imparting a torque on the spacecraft. Overall, the results presented here show promise for spherical actuator based attitude control systems.

REFERENCES

[1] Rossini, L., Chételat, O., Onillon, E., and Perriard, Y., "Analytical and Experimental Investigation on the Force and Torque of a Reaction Sphere for Satellite Attitude Control," *IEEE/ASME International Conference on Advanced Intelligent Mechatronics*, 2011.

[2] Rossini, L., Chételat, O., Onillon, E., and Perriard, Y., "Force and Torque Analytical Models of a Reaction Sphere Actuator Based on Spherical Harmonic Rotation and Decomposition," *IEEE/ASME Transactions on Mechatronics*, Vol. 18, No. 3, 2013, pp. 1006–18.

[3] Heinrich, C. R., "Spherical-Flywheel Attitude-Control System," 1961.

[4] Ormsby, R. D. and Smith, M. C., "Capabilities and Limitations of Reaction Spheres for Attitude Control," *ARS Journal*, Vol. 31, 1961, pp. 808–12.

[5] Tierney, T. and Curran, R., "Development of an Electrostatic Suspension Reaction Sphere," *Society of Automotive Engineers*, 1964.

[6] Davey, K., Vachtsevanos, G., and Powers, R., "The Analysis of Fields and Torques in Spherical Induction Motors," *IEEE Transactions on Magnetics*, Vol. 23, No. 1, 1987, pp. 273–82.

[7] Ruan, J., Huang, S., and Zhou, K., "Computation of 3D Electromagnetic Field and Torques in Spherical Motors," *The International Journal for Computation and Mathematics in Electrical and Electronic Engineering*, Vol. 17, 1998, pp. 106–110.

[8] Dehez, B., Galary, G., Grenier, D., and Raucent, B., "Development of a Spherical Induction Motor with Two Degrees of Freedom," *IEEE Transactions on Magnetics*, Vol. 42, No. 8, 2006, pp. 2077–89.

[9] Hosny, W. M. and Dodds, S. J., "Analytical Investigation of the Torque Capability of the Reaction Sphere," *Electric Machines and Power Systems*, 2007.

[10] Hu, Y., Chen, J., and Ding, X., "Analysis and Computation on Magnetic Field of Solid Rotor Induction Motor," *IEEE Transactions on Applied Superconductivity*, Vol. 20, No. 3, 2010.

[11] Iwakura, A., "Feasibility Study on Three Dimensional Reaction Wheel," *Proceedings of the School of Science of Tokai University*, Vol. 33, 2008, pp. 51–57.

[12] Shirasawa, Y. and Tsuda, Y., "Experimental Study and Analysis on Three Dimensional Reaction Wheel for Microsatellites," *Proceedings of the AAS/AIAA Space Flight Mechanics Meeting*, Vol. 130, 2008, pp. 507–17.

[13] Rossini, L., Chételat, O., Onillon, E., and Perriard, Y., "An Open-loop Control Strategy of a Reaction Sphere for Satellite Attitude Control," *International Conference on Electrical Machines and Systems*, 2011.

[14] Onillon, L. R. E., Chételat, O., and Perriard, Y., "An Optimal Sensor Placement Strategy for Force and Torque Analytical Models of a Reaction Sphere Actuator for Satellite Attitude Control," *Proceedings of the 2012 International Conference on Electrical Machines*, 2012, pp. 2545–51.

[15] Rossini, L., Mingard, S., Boletis, A., Forzani, E., Onillon, E., and Perriard, Y., "Rotor Design Optimization for a Reaction Sphere Actuator," *IEEE Transactions on Industry Applications*, Vol. 50, No. 3, 2014, pp. 1706–16.

[16] Rossini, L., Onillon, E., Chételat, O., and Perriard, Y., "Back-EMF and Rotor Angular Velocity Estimation for a Reaction Sphere Actuator," *IEEE/ASME International Conference on Advanced Intelligent Mechatronics*, 2014, pp. 334–9.

[17] Strumik, M., Wawrzaszek, R., Banaszkiewicz, M., Seweryn, K., Sidz, M., Onillon, E., and Rossini, L., "Analytical Model of Eddy Currents in a Reaction Sphere Actuator," *IEEE Transactions on Magnetics*, Vol. 50, No. 6, 2014.

[18] Schaub, H. and Junkins, J. L., *Analytical Mechanics of Space Systems*, AIAA Education Series, Reston, VA, 3rd ed., 2014.

[19] Tsiotras, P., "A Passivity Approach to Attitude Stabilization Using Nonredundant Kinematic Parameterizations," *Proceedings of the 34th IEEE Conference on Decision and Control*, Vol. 1, 1995, pp. 515–20.

APPENDIX: ALGEBRAIC FORCE AND TORQUE EXPRESSIONS

If the rotor is centered in the stator, explicit expressions for $\mathbf{F}_k$ and $\mathbf{T}_k$ exist and are given by

$$\mathbf{F}_k = \frac{i_k N}{A} \begin{pmatrix} \frac{\mu_0 \|\mathbf{m}\| (\ln(R_a) - \ln(R_b)) \left(\sin(\theta_a)^3 - \sin(\theta_b)^3\right) (C_{31}\cos(\beta)\sin(\alpha) - C_{33}\cos(\alpha) + C_{32}\sin(\alpha)\sin(\beta))}{4} \\ \frac{\mu_0 \|\mathbf{m}\| (\ln(R_a) - \ln(R_b)) \left(\sin(\theta_a)^3 - \sin(\theta_b)^3\right) (C_{32}\cos(\beta) - C_{31}\sin(\beta))}{4} \\ -\frac{\mu_0 \|\mathbf{m}\| (\ln(R_a) - \ln(R_b)) \left(\sin(\theta_a)^3 - \sin(\theta_b)^3\right) (C_{33}\sin(\alpha) + C_{31}\cos(\alpha)\cos(\beta) + C_{32}\cos(\alpha)\sin(\beta))}{2} \end{pmatrix}$$

$$\mathbf{T}_k = \frac{i_k N}{A} \begin{pmatrix} -\frac{\mu_0 \|\mathbf{m}\| (R_a - R_b)(2\theta_a - 2\theta_b - \sin(2\theta_a) + \sin(2\theta_b)) (C_{32}\cos(\beta) - C_{31}\sin(\beta))}{8} \\ \frac{\mu_0 \|\mathbf{m}\| (R_a - R_b)(2\theta_a - 2\theta_b - \sin(2\theta_a) + \sin(2\theta_b)) (C_{31}\cos(\beta)\sin(\alpha) - C_{33}\cos(\alpha) + C_{32}\sin(\alpha)\sin(\beta))}{8} \\ 0 \end{pmatrix}$$

where α and β are the latitude and longitude of the coil of interest with respect to the spacecraft body frame.